Biointerface Research in Applied Chemistry
Open-Access Journal (ISSN: 2069-5837)

Article
Volume 13, Issue 6, 2023, 553
https://doi.org/10.33263/BRIAC136.553

The Effect of Li_2O/K_2O Ratio on the Electrical and Dielectric Properties of Li_2O-K_2O-MoO_3-P_2O_5 Glasses

Asmae Er-Rafai [1], Mohamed Laourayed [1], Yasmina Alaoui [1], Mouloud El Moudane [1,*], Nour-Eddine Lazar [2], Abdellah Benzaouak [2], Abdelkbir Bellaouchou [1]

[1] Laboratory of Materials, Nanotechnology, and Environment, Faculty of Sciences, Mohammed V University in Rabat, P.O. Box. 1014, Agdal-Rabat, Morocco
[2] Laboratory of Spectroscopy, Molecular Modeling, Materials, Nanomaterials, Water and Environment, Materials for Environment Team, ENSAM, Mohammed V University in Rabat, Morocco
* Correspondence: m.elmoudane@gmail.com (M.E.);

Scopus Author ID 56094483400
Received: 3.11.2022; Accepted: 11.01.2023; Published: 24.02.2023

Abstract: The influence of Li_2O/K_2O ratio on the electrical and dielectric properties of xLi_2O-$(25-x)K_2O$-$25MoO_3$-$50P_2O_5$ glasses with x values varying from 0 to 20 was reasonably evaluated. The structural characterization of the synthesized glasses using FTIR and Raman spectroscopies suggests that the substitution of Li_2O by K_2O changes the network's structure. Indeed, the results show the establishment of a more open system and facilitate the movement of the charge carriers (Li^+) through the network, showing a decrease in the activation energy. Consequently, Li^+ ions generate bonding defects in the glassy lattice, leading to a growth in the dielectric parameters. Thus, the conductivity's temperature dependency indicates the glasses' semiconducting character.

Keywords: glasses; phosphate; lithium oxide; dielectric constant; dielectric loss; conductivity.

1. Introduction

Phosphate glasses have potentially compelling properties that can be used in various applications because of their distinct physical properties, including hardness, more significant thermal expansion coefficient, low glass transition temperature, and reduced melting temperature. They are attractive targets for the manufacture of solid electrolytes and amorphous semiconductors. They are preferred materialsor high-power laser, optoelectronic, nuclear waste storage applications, high UV transmission, and electrical conductivity [1–12]. Phosphate glasses have recently seen a significant increase in use in the field of electronics thanks to their superior mechanical durability, optical transparency, and excellent thermal and chemical stability when compared to silicate- or borate-based materials. These glasses have numerous benefits and high ionic conductivity, including the lack of grain boundaries, isotropic properties, manufacturing simplicity, and stability improvement [6].

On the other hand, significant variability in the composition of oxide glasses proposes prospects for combining ionic conduction with electronic transport by introducing transition metal oxides (TMO) such as MoO_3, WO_3, V_2O_5, or Fe_2O_3 [13–15]. Depending on their concentration, molybdenum cations can act as both a network former and a network modifier [16–18]. The modification of Phosphate glasses properties occurs by adding halides or oxides of alkali, alkaline earth, and transition metals in the glass network [8]. Therefore, the structural network is altered by doping them with other elements' traces, namely alkali metals (Li+), which boost their ionic conductivity and make them useful for solid-state technology [19–25]. High ionic conductivity glasses are attracting researchers' interest due to their varied applicability for solid electrolytes in electrochemical instruments, including advanced energy density batteries and sensors [26].

Song *et al*. [27] investigate the effect of MAE on the DC electrical conductivity and structural and optical properties of $40P_2O_5$-$10MnO_2$-$(_{50-x})$ Li_2O-xK_2O phosphate glasses. Garrigou-lagra *et al*. [28] demonstrated that In the Li2O-Cd0-P205 ternary system, the Li_2O oxide acts as a structure modifier, like all alkali oxides. The study of the system Li_3PO_4–$Pb_3(PO_4)_2$–$BiPO_4$ (Li_2O–PbO–Bi_2O_3–P_2O_5) by El Moudane *et al*. [29] discovered that the ionic conductivity, σ, increases substantially with increasing concentration of lithium oxide. The study of lithium metaphosphate glasses of the series (100-x) Li_2O - xCu_2O - $50P_2O_5$ suggests that by replacing Li_2O with Cu_2O, the electrical conductivity decreases, and the activation energy increases, as in a typical mobile ion mixing effect [30].

In a previous paper, a study of the Molybdenum oxide's influence on the structural and thermal properties and the chemical dissolution of (50-x) K_2O-$xMoO_3$-$50P_2O_5$ phosphate-based glasses, varying x from 0 to 40 mol% molybdenum oxide was performed [18]. Li_2O was picked for insertion in the chosen glass system due to the noteworthy distinction in ionic radii and atomic masses of both lithium and potassium. The influence of the Li_2O/K_2O ratio on the electrical and dielectric properties of the quaternary system xLi_2O-$(_{25-x})$ K_2O-$25MoO_3$-$50P_2O_5$ was analyzed.

2. Materials and Methods

A specific composition xLi_2O-$(_{25-x})$ K_2O-$25MoO_3$-$50P_2O_5$, including five x values ranging from 0 to 20, was prepared for the current investigation. The samples were prepared from a chemical mixture of $NH_4H_2PO_4$, $(NH_4)_6Mo_7O_{24}.4H_2O$, K_2CO_3, and Li_2CO_3 of high reagent grade purity (Sigma-Aldrich) with precise proportions for each composition operating the traditional melt-quenching method. Before, the mixture gradually grew to the melting temperature between 700–800 ◦C and was fixed for 1 hour. The composition details selected for the current investigation are depicted in Table 1.

The complexity of glass alteration mechanisms requires macroscopic and microscopic characterization of the altered glasses. Therefore, X-ray diffraction was used to highlight the presence or absence of crystalline phases in the glasses. This analysis was achieved through a D5000 Siemens diffractometer λ=0.5418 nm with a scanning rate of 2° from 5° to 90°. Glass density measurements were performed via the Archimedes technique using diethyl phthalate as immersion fluid at 25 °C. We present a structural investigation combining spectroscopy techniques such as FT-IR and Raman to assess these vitreous materials’ structure as a function of composition. Following the approach of another previous work, we carried out these techniques [18]. In the frequency range of 4000–400 cm^{-1}, the FTIR parameters were determined using a Jasco 4600 FTIR spectrometer with an instrumental resolution of 4 cm^{-1}. Following the approach of another previous work, we carried out these techniques. Also, Raman spectrums were acquired at ambient temperature via a Renishaw RM1000 Raman micro-spectrometer linked to a red He-Ne laser (19 mW) with a 632.8 nm line. The spectrum was taken between 200 and 1400 cm^{-1}.

Five specimens were carved and perfectly polished into the shape of two-sided parallel disks. Then, place a tiny layer of gold paste on the opposing faces. The disk was positioned between the platinum electrodes to guarantee a correct electrical connection. They were using a HIOKI 3532-50 HiTESTER LCR in the temperature ranging between 25-300 °C and a frequency of 15-30 kHz to estimate the samples' dielectric constant (Ɛ'), ionic conductivity (σ), and dielectric loss tangent (tan δ).

3. Results and Discussion

3.1. X-ray analysis, density, and molar volume.

Peaks' absence in the XRD spectra confirms the materials' amorphous character (Figure 1). The density and molar volume measurements of the five glass samples as a function of the Li_2O/K_2O ratio are shown in Table 1 and Figure 2. The density of the studied glasses series decreases with the Li2O/K2O ratio increase from 3.64 g.cm^{-3} (x = 0 mol %) to 3.08 g.cm-3 (x = 20 mol %). In contrast, the molar volume increases from 35.85 cm3.mol-1 (x = 0 mol %) to 38.19 cm3.mol-1 (x = 20 mol %). These changes are due to the difference in Density between Li+ and K+ (0.534 g.cm-3 and 0.89 g.cm-3, respectively). Thus, the atomic mass of K+ is higher than that of Li+.

It should be noted that the density presents a nonlinear variation with Li_2O/K_2O. This can be explained by the functioning of the MAE in the present glassy system [27]. Many glasses containing alkali metal oxides show nonlinear variations in their physical properties when another progressively replaces one alkali metal oxide. This phenomenon is known as the mixed alkali effect (MAE). The MAE is important concerning ionic transport properties, such as electrical conductivity, activation energy, dielectric loss, glass transition temperature, internal friction, viscosity, and density. The MAE becomes stronger with increasing total alkali metal ion concentration and cation size shift.

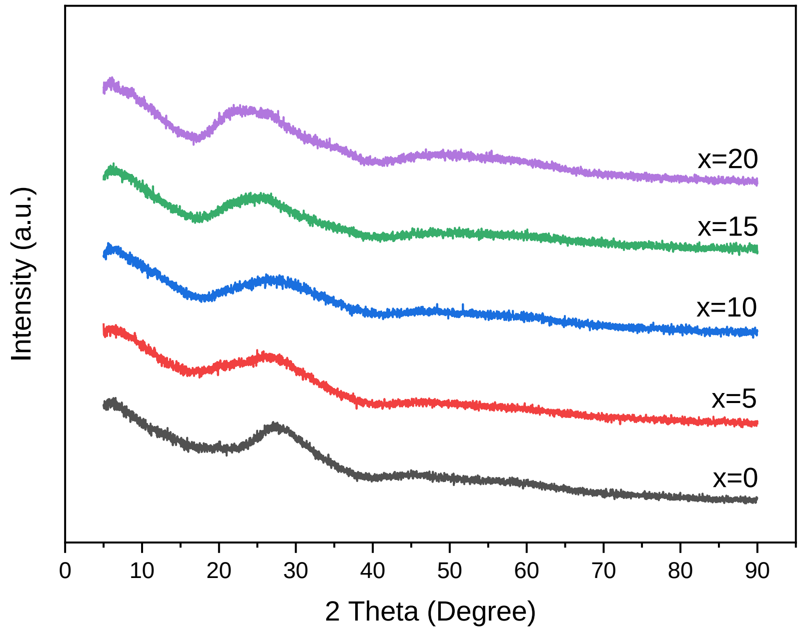

Figure 1. The Diffractograms of xLi_2O-(25-x) K_2O-25MoO_3-50P_2O_5 compositions.

Table 1. Physical parameters of xLi_2O-(25-x) K_2O-25MoO_3-50P_2O_5 glasses.

x	Composition (mol %)				Li_2O/K_2O ratio	ρ (g.cm^{-3})	V_M (cm^3.mol^{-1})
	Li_2O	K_2O	MoO_3	P_2O_5			
0	0	25	25	50	0.00	3.64	35.85
5	5	20	25	50	0.25	3.50	36.36
10	10	15	25	50	0.67	3.36	36.92
15	15	10	25	50	1.50	3.20	37.76
20	20	5	25	50	4.00	3.08	38.19

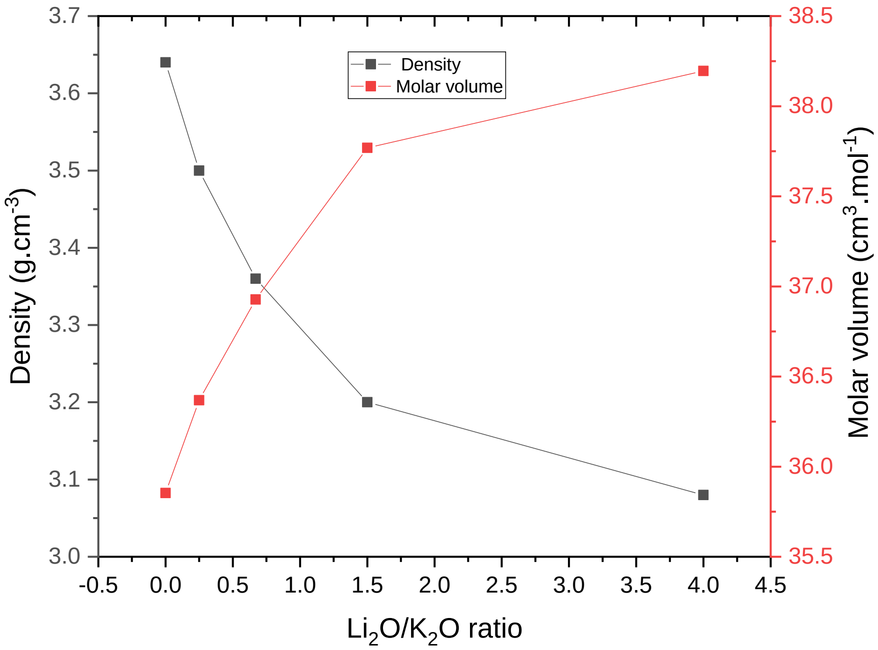

Figure 2. Variation of densities and molar volumes for $xLi_2O-(25-x) K_2O-25MoO_3-50P_2O_5$glasses as a function of Li_2O/K_2O ratio.

3.2. FT-IR and Raman spectroscopies.

Figure 3 shows all glasses' IR spectra between 400 and 1400 cm^{-1}. Their characteristics attributed according to the literature are: the symmetric νs(PO2) stretching modes at 1150 cm^{-1}[31], the peaks of absorption at 950-900 cm-1 are ascribed to the νas (P-O-P) [32], the bands at 840-700 assigned to the asymmetric stretching vibration of P-O-P groups in PO_4 structural units (νs(P-O-P)) [33, 34] and the bending vibrations (δ) of P – O- bonds at 630 cm^{-1}-550 cm^{-1} [1]. In FTIR spectra, specific vibrations of Li-O appeared around 415 cm^{-1} [35]. All these glasses present the same bands. However, their intensities decrease by increasing the Li2O/K2O ratio, suggesting that introducing lithium alters the network's structure [26].

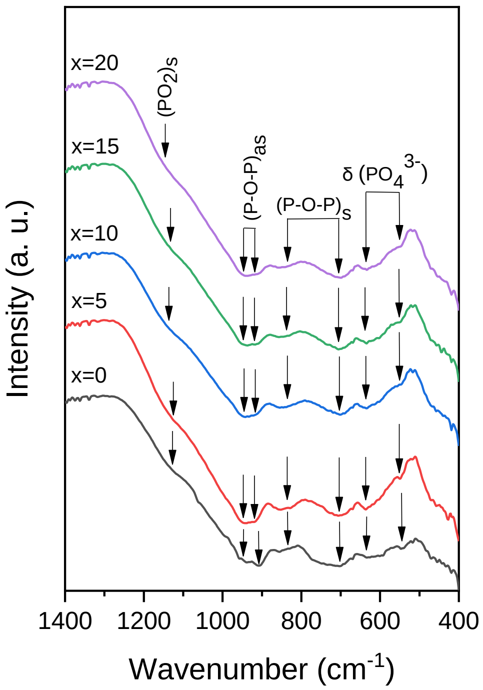

Figure 3. IR Spectra of $xLi_2O-(25-x) K_2O-25MoO_3-50P_2O_5$ glasses.

Figure 4 shows the Raman spectrum of xLi_2O-(25-x) K_2O-25MoO_3-50P_2O_5 glasses, registered in the frequency ranging from 100 to 1200 cm-1. All the spectra are characterized by seven vibrational bands at 1070, 930, 840, 750, 570, 480, and 320 cm-1. The classification of phosphate structural groups is represented by the formula Qn, where n is the number of bridging oxygens (BOs) per unit. Depending on the type and concentration of the glass modifier, the structural groups of phosphate glasses move from ultraphosphate (Q3) to metaphosphate (Q2), pyrophosphate (Q1), and orthophosphate (Q0) [36, 37].

According to the literature, the first bands are due to the symmetric stretching vibrations (PO2) units ((υas (PO2), (Q2)) [1, 38–41]. The asymmetric and symmetric stretching vibration POP of non-bridging oxygen in PO_4 tetrahedron units in Q1 groups (υas (P-O-P) and υs (P-O-P), (Q1)) are around 930-840 cm^{-1} [23] and 750-570 cm^{-1} [24]. However, the last two bands are ascribed as modes' deformation of P-O- (PO_4^{3-}) groups in isolated Q0 phosphate tetrahedral units [38, 40, 42] overlapped with the vibrational mode of LiO_4 tetrahedron occurs in the range 350–500 cm^{-1} [43] making their distinction is not simple to discern. At the same time, the vibrational mode of LiO_6 octahedron appears at lower wavenumbers in the range 200–300 cm^{-1} [44, 45]. Nevertheless, phosphate lattice changes are reflected in investigated spectra by the intensity of the bands, which increases with the lithium concentration. Therefore, doping the glass with Li_2O resulted in the breakage of the weaker P-O-K bond, creating a stronger P-O-Li bond [46], creating bridging oxygen in the system [47].

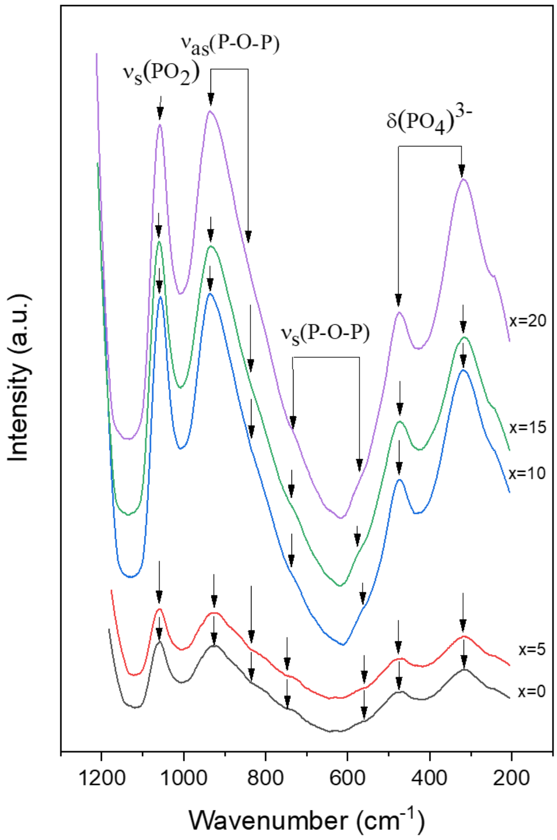

Figure 4. Raman spectra of xLi_2O-(25-x) K_2O-25MoO_3-50P_2O_5 glasses.

3.3. Dielectric constant (ε') and Dielectric loss (tanδ).

Based on the measurements of the capacitance C, the dielectric constant (ε') is deduced as:

$$\varepsilon' = \frac{C.d}{\varepsilon_0.A}$$

where ($\varepsilon\mathbf{0}$) is the free space permittivity, (C) is the capacitance, (d) is the sample thickness, and (A) is the cross-sectional area of the specimen. Figure 5 shows the evolution of the dielectric constant (ε') as a function of temperature at different frequencies of the various compositions studied. Note that the same trend was observed for all the frequencies investigated: (a) 15 KHz, (b) 20 KHz, (c) 25 KHz, and (d) 30 KHz; the values of the constant dielectric increase with increasing temperature. The electronic and ionic constituents' contributions to overall polarization will be negligible at low temperatures [48]. Temperature rising underlines the significant impact of charges thermally activated, for example, charged defects, space charges, and associated complex defects [49]. The increasing rate of (ε') with temperature is most remarkable for glasses containing the highest concentration of Li_2O. The dielectric constant is almost independent of temperature below 500 ◦C and shows little frequency dispersion. However, it shows strong temperature dependence and frequency dispersion above this temperature.

Meanwhile, the dielectric constant's variation (ε') of xLi_2O-$(_{25-x})$ K_2O-$25MoO_3$-$50P_2O_5$ glasses as a temperature at different percentages of Li_2O is shown in Figure 6.

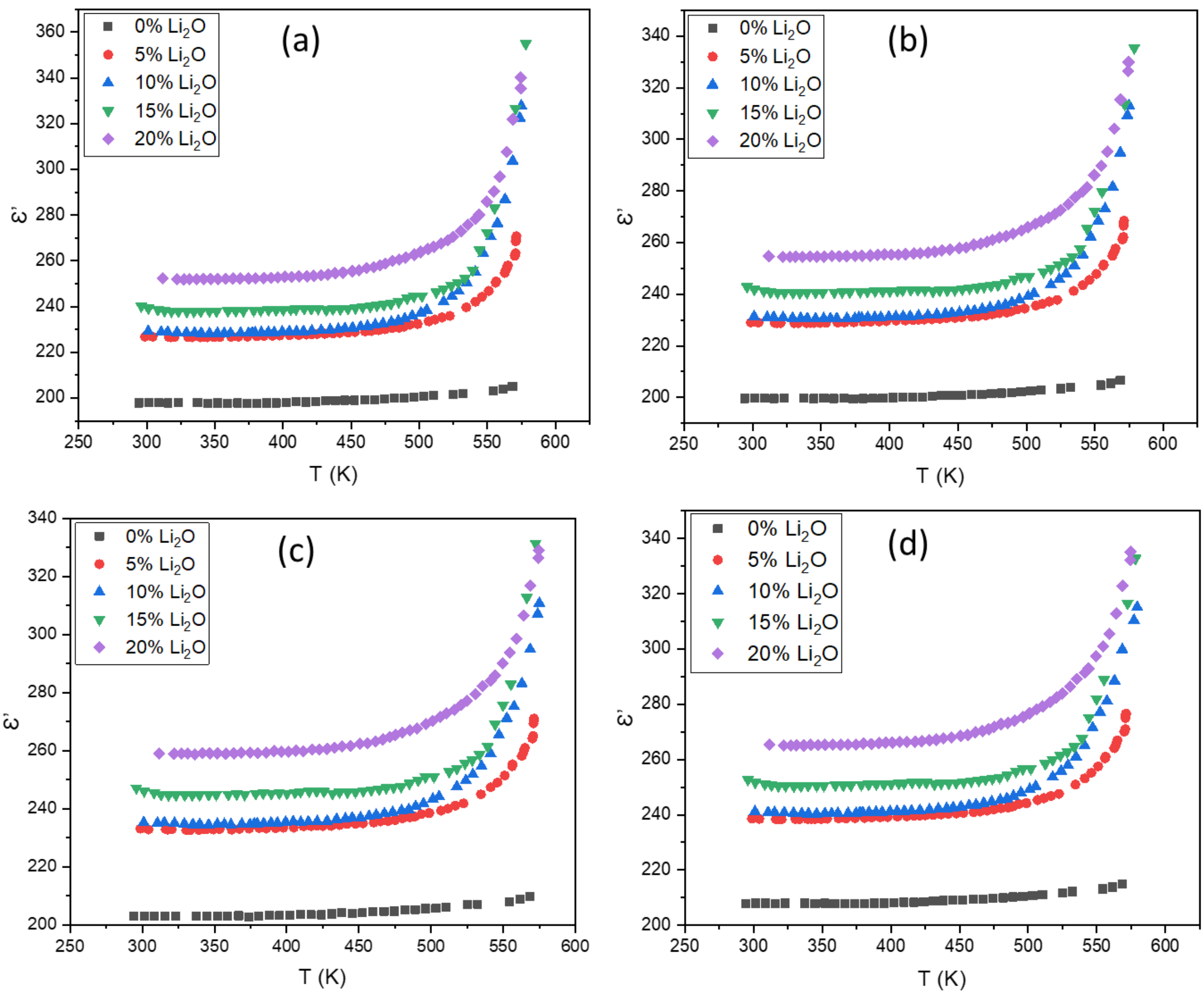

Figure 5. The dielectric constant (ε') as a function of temperature at various frequencies: **(a)** 15 KHz, **(b)** 20KHz, (c) 25 KHz et (d) 30 KHz of xLi_2O-(25-x) K_2O-$25MoO_3$-$50P_2O_5$ glasses.

All compositions: (a) 0% Li_2O, (b) 5% Li_2O, (c) 10% Li2O, (d) 15% Li_2O, and (e) 20% Li_2O, show the same behavior. The large values of the dielectric constant are obtained at higher frequencies as the temperature rises. It should also be noted that by increasing the percentage of Li2O, the effect of increasing the frequency decreases. With Koop's phenomenological theory, the Maxwell-Wagner two-layer model can explain the variation of the dielectric constant (ε') with frequency. Based on this model, dielectric materials consist of many well-conducting grains that are isolated by joints of thin, poorly-conducting grains. Introducing an exterior electric field moves the charge carriers readily from the grains and collects them at the grain borders, thus generating a significant polarization and many dielectric invariants [50].

As well as the dielectric constant (ε'), the dielectric loss ($tan\delta$) shows a considerable increase as a function of temperature with increasing frequency Figure 7 (a) and with the substitution of K_2O by Li_2O Figure 7 (b). This trend can be attributed to the fact that Li_2O ions serve in the glass lattice as modifiers generating bonding deficiencies and increasing the dielectric parameters [51]. The same behavior was noticed for all compositions and measurement frequencies. The dielectric loss is high and then increases frequency increases. This high dielectric loss is due to more number of drifting charge carriers. At high temperatures, the effect of frequency on dielectric losses is significant. This is attributed to the thermal effect on the charge carriers' drift rate and jump frequency, which increases the dielectric losses.

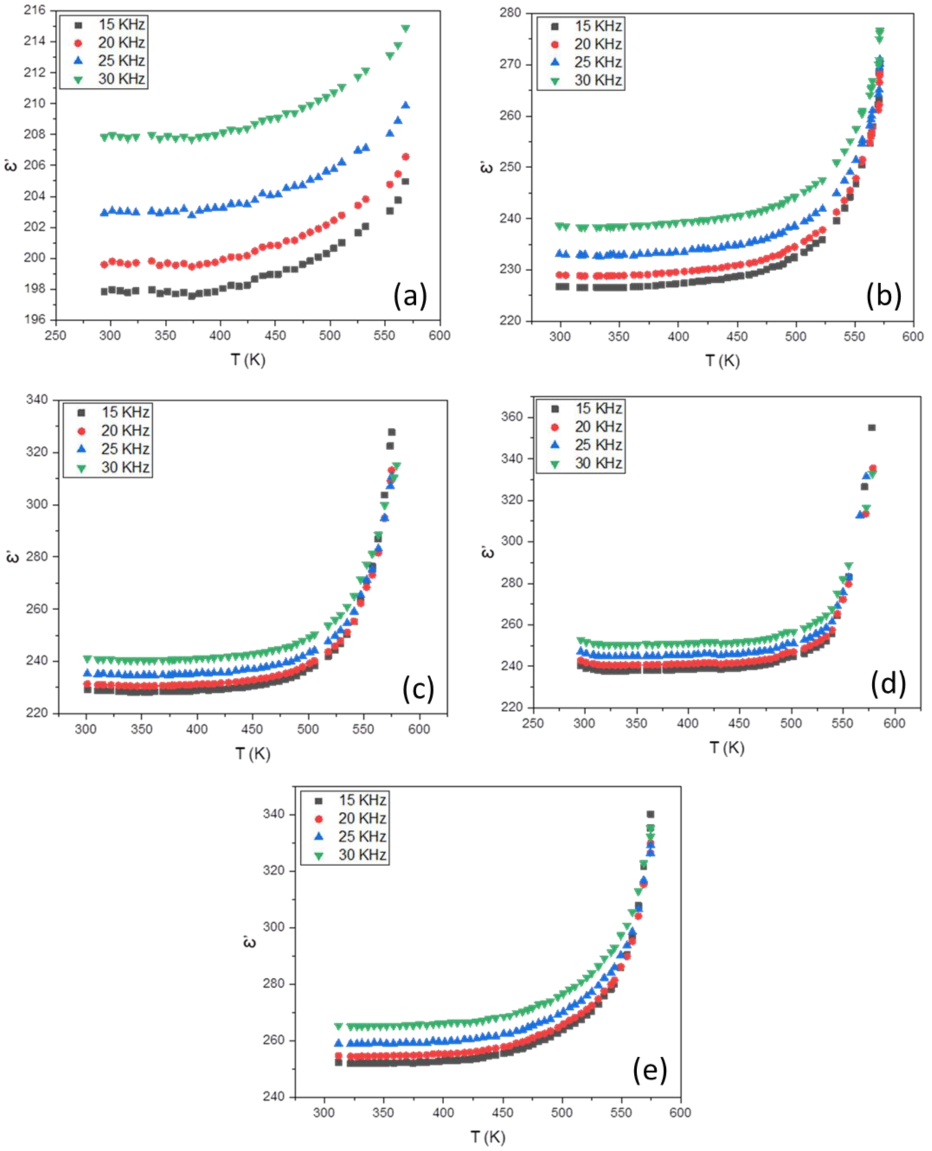

Figure 6. The dielectric constant (ε') as a function of temperature at different percentages of Li_2O: **(a)** 0%, **(b)**5%, **(c)** 10%, **(d)** 15% et **(e)** 20% of xLi_2O-(25-x) K_2O-25MoO_3-50P_2O_5 glasses.

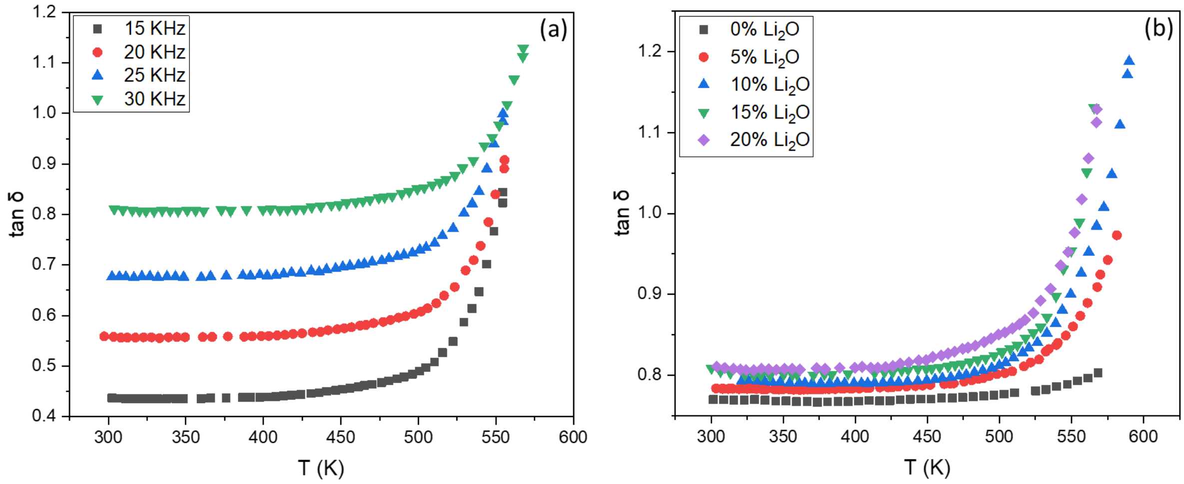

Figure 7. The Dielectric loss ($tan\delta$) with the temperature at **(a)**20% of Li_2O, **(b)** 30 kHz ofxLi_2O-(25-x) K_2O-25MoO_3-50P_2O_5 glasses.

3.4. AC conductivity (σ_{ac}).

The AC conductivity of all the glasses (σac) is given by:

$$\sigma ac = \varepsilon 0 \omega \varepsilon' \tan\delta$$

where ε0 the permittivity of free space, ω(=2πf) is the angular frequency, ε' is the dielectric constant, and tanδ is the dielectric loss. Figure 8 depicts the conductivity temperature dependency of the examined glasses. According to the results, the conductivity increases with increasing temperature, indicating the semiconducting nature of glasses[33, 48, 52]. The best conductivity is presented by the composition containing the highest percentage of Li2O (20%) and increases with increasing frequency. This variation can be attributed to the movement of Li+ ions within the glass network. It is well known in the literature that, in oxide glasses, the conductivity increases as the size of the charge carrier decreases [8]. This is consistent with the replacement of K2O with Li2O throughout this case.

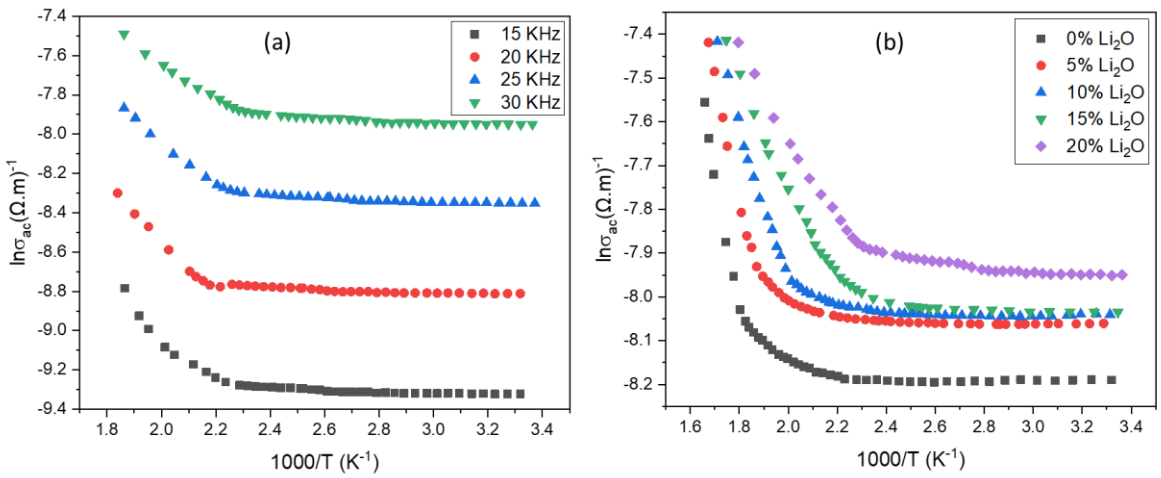

Figure 8. Thea.c. conductivity σ_{ac} with $10^3/T$ at: **(a)** 20% of Li_2O, **(b)** 30 KHz of xLi_2O-(25-x) K_2O-25MoO_3-50P_2O_5 glasses.

The Arrhenius equation is used to compute the activation energy for the glassy specimens based on the measurement results in Figure 8:

$$\sigma = \sigma 0.\exp (Ea/kBT)$$

where σ is the conductivity, σ0 is the pre-exponent's conductivity, Ea is AC conductivity's activation energy, kB is the Boltzmann constant, and T is the temperature. The variation of the activation energy (Figure 9 and Table 2) shows a decrease with the addition of Li_2O. Indeed, incorporating a modifying oxide (Li_2O) in the glassy network helps form a more open structure and facilitates the movements of the charge carriers (Li^+) through the network. Thus, the addition of Li_2O minimizes the potential energy barriers to be overcome by the mobile ion in its jumps [53].

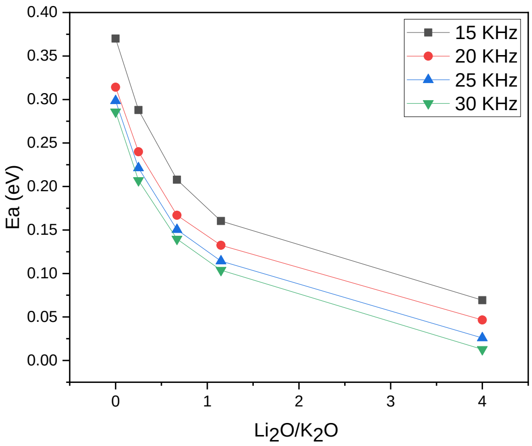

Figure 9. Activation energy with Li_2O/K_2O ratio at different frequencies.

Table 2. The activation energy values with Li_2O/K_2O ratio at different frequencies.

Li_2O/K_2O	**Ea (eV)**			
	15 KHz	**20 KHz**	**25 KHz**	**30 KHz**
0	0.3701	0.31415	0.29847	0.28583
0.25	0.28794	0.2399	0.22134	0.20693
0.67	0.20778	0.16694	0.15029	0.13968
1.15	0.16027	0.13244	0.1142	0.10377
4	0.06934	0.04651	0.02588	0.01278

4. Conclusions

The structural alterations in the examined amorphous system were caused by doping with additional elements, such as alkali oxides (Li^+ in this example). The increasing Li_2O/K_2O ratio leads to breaking the weaker P-O-K bond and forming a stronger P-O-Li bond. Meanwhile, the increase in dielectric parameters can be attributed to the modifier role of Li_2O, which induce bonding defects in the glassy lattice. The conductivity temperature dependency of the studied glasses indicates their semiconducting nature. Thus, adding Li_2O allows the formation of a more open structure, facilitates the movement of charge carriers (Li^+) through the lattice, and minimizes the potential energy barriers. As a result, the activation energy is reduced.

Funding

This research received no external funding.

Acknowledgments

We thank all our colleagues.

Conflicts of Interest

The authors declare no conflict of interest.

References

1. El Hezzat, M.; Et-Tabirou, M.; Montagne, L.; Bekaert, E.; Palavit, G.; Mazzah, A.; Dhamelincourt, P. Structure and ac conductivity of sodium–lead–cadmium metaphosphate glasses. *Mater. Lett.* **2004**, *58*, 60-66, https://doi.org/10.1016/S0167-577X(03)00415-4.
2. Laourayed, K.; El Moudane, M.; Khachani, M.; Shaim, A.; Boudalia, M.; Sabbar, A.; Ghanimi, A.; Guenbour, A.; Bellaouchou, A. Preparation, and study of dielectric proprieties of glassy materials in ternary system Bi_2O_3-Nb_2O_5-P_2O_5. *Mater. Today: Proc.* **2020**, *22*, 108–111, https://doi.org/10.1016/j.matpr.2019.08.108.
3. Jerroudi, M.; Biha, L.; Haily, E.; Yousfi, S.; Bejjit, L.; Haddad, M.; Manoun, B.; Lazor P. Optical and electrical properties of manganese doped-alkali metaphosphate glasses. *Mater. Today: Proc.* **2020**, *30*, 1052–1055, https://doi.org/10.1016/j.matpr.2020.04.765.
4. Little Flower, G.; Sahaya Baskaran, G.; Srinivasa Reddy, M.; Veeraiah, N. The structural investigations of PbO–P_2O_5–Sb_2O_3 glasses with MoO_3 as additive by means of dielectric, spectroscopic and magnetic studies. *Physica B* **2007**, *393*, 61–72, https://doi.org/10.1016/j.physb.2006.12.070.
5. Ahmina, W.; El Moudane, M.; Zriouil, M.; Cherraj, M.; Taibi, M. Study of the mechanical and chemical properties of potassium manganese phosphate glasses. *Matec Web Of Conferences* **2018**, *149*, 01081, https://doi.org/10.1051/matecconf/201814901081.
6. Ahmina, W.; El Moudane, M.; Shaim, A.; Zriouil, M.; Taibi, M. Chemical durability, electrical and dielectric properties of the ternary system (50-x)K_2O-xMnO-50P_2O_5 phosphate glasses. *Mater. Today: Proc.* **2019,** *13*, 466-473, https://doi.org/10.1016/j.matpr.2019.04.003.
7. Ahmina, W.; El Moudane, M.; Zriouil, M.; Taibi, M. Effect of the content of MnO on the electric-dielectric properties of potassium phosphate glasses. *J. Mater. Environ. Sci.* **2017**, *11*, 4193-4198, https://www.jmaterenvironsci.com/Document/vol8/vol8_N11/440-JMES-3573-Ahmina.pdf.
8. Mugoni, C.; Montorsi, M.; Siligardi, C.; Jain, H. Electrical conductivity of copper lithium phosphate glasses, *J Non Cryst Solids* **2014**, *383*, 137–140, https://doi.org/10.1016/j.jnoncrysol.2013.04.048.
9. El-Damrawi, G.; Abdelghany, A. M.; Madshal, M. A. AC conductivity and dielectric properties of Cr_2O_3 doped SrO–P_2O_5 glasses. *Physica B* **2021**, *618*, 413184, https://doi.org/10.1016/j.physb.2021.413184.
10. Assad, H.; Kharroubi, M. Dielectric studies and Cole-Cole plot analysis of Na_2O–(1-x)ZnO–xCoO–P_2O_5 glasses. *J. Non-Cryst. Solids* **2021**, 560, 120721, https://doi.org/10.1016/j.jnoncrysol.2021.120721.
11. Mokhtar, K.; Mohamed, K.; Lakhdar, G.; Sébastien, B.; Hamza, A. Electrical conductivity and dielectric properties of rare earth ions (Ce^{3+}, Pr^{3+} and Eu^{3+}) doped in zinc sodium phosphate glass. *J. Non-Cryst. Solids* **2021**, *567*, 120933, https://doi.org/10.1016/j.jnoncrysol.2021.120933.
12. Kassa, B.; Leta Tesfaye, J.; Bulcha, B.; Kiran, R.; Deepak, T.; Lal, D.; Venkatesh, S.; Krishnaraj, R.Effect of Manganese Ions on Spectroscopic and Insulating Properties of Aluminophosphate Glasses. *Adv. Mater. Sci. Eng.* **2021**, *2021*, https://doi.org/10.1155/2021/6253069.
13. Pavić, L.; Šantić, A.; Nikolić, J.; Mošner, P.; Koudelka, L.; Pajić, D.; Moguš-Milanković, A. Nature of mixed electrical transport in Ag_2O–ZnO–P_2O_5 glasses containing WO_3 and MoO_3. *Electrochim. Acta* **2018**, *276*, 434-445, https://doi.org/10.1016/j.electacta.2018.04.029.
14. Mohamed, S. N.; Halimah, M. K.; Subban, R. H. Y.; Yahya, A. K. AC conductivity and dielectric properties in mixed ionic–electronic 20Na_2O–20CaO–(60–x)B_2O_3–xV_2O_5 glasses. *Physica B* **2021**, *602*, 412480, https://doi.org/10.1016/j.physb.2020.412480.
15. Ramadan, R. M.; Hammad, A. H.; Wassel, A. R. Impact of copper oxide on the structural, optical, and dielectric properties of sodium borophosphate glass. *J. Non-Cryst. Solids* **2021**, *568*, 120961, https://doi.org/10.1016/J.JNONCRYSOL.2021.120961.
16. Lynch, G. F.; Sayer, M.; Segel, S. L.; Rosenblatt, G. Electron and nuclear magnetic resonance in semiconducting phosphate glasses. *J. Appl. Phys.* **1971**, *42*, 2587–2591, https://doi.org/10.1063/1.1660593.
17. Selvaraj, U.; Rao, K. J. Characterization studies of molybdophosphate glasses and a model of structural defects. *J. Non-Cryst. Solids* **1985**, *72*, 315-334, https://doi.org/10.1016/0022-3093(85)90187-5.
18. Er-Rafai, A.; El Moudane, M.; Alaoui, Y.; Laourayed, M.; Taibi, M.; Warad, I.; Guenbour, A.; Bellaouchou, A.; Zarrouk, A. Effect of Molybdenum Oxide on Structural Characteristics, Thermal Properties, and

Chemical Dissolution of (50-x)K_2O-xMoO_3-50P_2O_5 Phosphate Glasses. *Biointerface Res. Appl. Chem.* **2023**, *13*, 294, https://doi.org/10.33263/BRIAC133.294.

19. Rani, S.; Sanghi, S.; Ahlawat, N.; Agarwal, A. Crystallization kinetics, optical and dielectric properties of $Li_2O{\cdot}CdO{\cdot}Bi_2O_3{\cdot}SiO_2$ glasses. *J. Mol. Struct* **2015**, *1098*, 1–11,https://doi.org/10.1016/J.MOLSTRUC.2015.05.017.
20. Shams, M. S.; Rammah, Y. S.; El-Agawany, F. I.; Elsad, R. A. Synthesis, structure, physical, dielectric characteristics, and gamma-ray shielding competences of novel P_2O_5–Li_2O–ZnO–CdO glasses. *J. Mater. Sci. Mater. Electron.* **2021**, *32*, 1877–1887, https://doi.org/10.1007/s10854-020-04956-6.
21. Sutrisno, M. S.; Samsudin, N. M.; Sazali, E. S.; Hisam, R. AC conductivity and dielectric properties of 98[20Li_2O-xBi_2O_3-(80-x)TeO_2]-2Ag mixed ionic-electronic glasses. *J. Mater. Sci. Mater. Electron.* **2021**, *32*, 5138–5155, https://doi.org/10.1007/s10854-021-05246-5.
22. Liang, T.; Zhang, J.; Chen, H.; Gao, L.; Qu, S.; Harris, V. G. Impact of alkaline earth oxides on dielectric properties of photoetchable glasses as interposers for integrated circuits packaging. *J. Alloys Compd.* **2021**, *874*, 159546, https://doi.org/10.1016/J.JALLCOM.2021.159546.
23. Boora, M.; Malik, S.; Kumar, V.; Bala, M.; Arora, S.; Rohilla, S.; Kumara, A.; Dalal, J. Investigation of structural and impedance spectroscopic properties of borate glasses with high Li^+ concentration. *Solid State Ionics* **2021**, *368*, 115704, https://doi.org/10.1016/J.SSI.2021.115704.
24. Monishaa, M.; Prabhua, N. S.; D'Souzaa, N.S.; Bharadwaj, S.; Chowdary, R. J.; Sayyed, M. I.; Alhuthalie, A.M. S.; Al-Hadeethif, Y.; Kamath, S.D. Structural, dielectric, optical and photoluminescence studies of Tm^{3+} doped B_2O_3-BaO-MgO-Li_2O-Na_2O-LiF glasses featuring strong blue emission. *J. Non-Cryst. Solids* **2021**, *560*, 120733, https://doi.org/10.1016/J.JNONCRYSOL.2021.120733.
25. Somaily, H. H.; Algarni, H.; Rammah, Y. S.; Alalawi, A.; Mutuwong, C.; Al-Buriahi, M. S. The effects of V_2O_5/K_2O substitution on linear and nonlinear optical properties and the gamma ray shielding performance of TVK glasses. *Ceram. Int.* **2021**, *47*, 1012–1020, https://doi.org/10.1016/J.CERAMINT.2020.08.215.
26. Rani, S.; Sanghi, S.; Ahlawat, N.; Agarwal, A. Influence of Bi2O3on physical, electrical and thermal properties of Li_2O-ZnO-Bi_2O_3-SiO_2 glasses. *J. Alloys Compd.* **2015**, *619*, 659–666, https://doi.org/10.1016/j.jallcom.2014.09.029.
27. Song, J.; Wu, D.; Zhang, C.; Ming, Q.; Imanzadeh, M. Investigation of mixed alkali effect on the DC electrical conductivity, structural, and physical properties of phosphate glasses containing MnO_2. *J. Phys. Chem. Solids* **2022**, *167*, 110759, https://doi.org/10.1016/j.jpcs.2022.110759.
28. Garrigou-Lagrange, C.; Ouchetto, M.; Elouadi, B. Infrared spectra of vitreous lithium and cadmium mixed phosphates. *Can. J. Chem.* **1985,** 63, 1436-1446.
29. Elmoudane, M.; Et-tabirou, M.; Hafid, M. Glass-forming region in the system Li_3PO_4–$Pb_3(PO_4)_2$–$BiPO_4$ (Li_2O–PbO–Bi_2O_3–P_2O_5) and its ionic conductivity. *Mater. Res. Bull.* **2000**, *35*, 279-287, https://doi.org/10.1016/S0025-5408(00)00196-3.
30. Mugoni, C.; Montorsi, M.; Siligardi, C.; Jain, H. Electrical conductivity of copper lithium phosphate glasses. *J. Non Cryst Solids* **2013**, *383*, 137–140, https://doi.org/10.1016/j.jnoncrysol.2013.04.048.
31. Wanga, F.; Wang, Y.; Zhang, D.; Hao, Y.; Liao, Q.; Zhu, H.; Zhoua, J.; Zhu, Y. Effects of MoO_3 and Nd_2O_3 on the structural features, thermal stability and properties of iron-boron-phosphate based glasses and composites. *J. Nucl. Mater.* **2022**, *560*, 153500, https://doi.org/10.1016/j.jnucmat.2021.153500.
32. Ahmina, W.; El Moudane, M.; Zriouil, M.; Taibi, M. Glass-forming region, structure and some properties of potassium manganese phosphate glasses. *Phase Transitions* **2016**, *89*, 1051–1061, https://doi.org/10.1080/01411594.2016.1144057.
33. Nagarjuna, M.; Satyanarayana, T.; Ravi Kumar, V.; Veeraiah, N. Ag concentration dependent transport properties of LiF-MoO_3-P_2O_5 glasses. *Phys. B* **2009**, *404*, 3748–3755, https://doi.org/10.1016/J.PHYSB.2009.06.123.
34. Dayanand, C.; Bhikshamaiah, G.; Tyagaraju, V. J.; Salagram, M.; Murthy, A. S. R. K. Review Structural investigations of phosphate glasses: a detailed infrared study of the x(PbO)-(1-x)P_20_5 vitreous system. *J. Mater. Sci.* **1996**, *31*, 1945-1967, https://doi.org/10.1007/BF00356615.
35. Samee, M. A.; Edukondalu, A.; Ahmmad, S. K.; Taqiullah, S. M.; Rahman, S. Mixed-alkali effect in Li_2O-Na_2O-K_2O-B_2O_3 glasses: Infrared and optical absorption studies. *J. Electron. Mater* **2013**, *42*, 2516–2524, https://doi.org/10.1007/S11664-013-2605-0.
36. le Saoût, G.; Simon, P.; Fayon, F.; Blin, A.; Vaills, Y. Raman and infrared study of (PbO)x(P2O5)(1-x) glasses. *J. Raman Spectrosc* **2002**, 740–746, https://doi.org/10.1002/jrs.911.

37. Burba, C. M.; Frech, R. Raman and FTIR Spectroscopic Study of Li_xFePO_4 (0≤x≤1). *J. Electrochem. Soc.* **2004**, *151*, A1032-A1038, https://doi.org/10.1149/1.1756885.
38. Alaoui, Y.; Laourayed, M.; Er-rafai, A.; Hammi, M.; El Moudane, M.; Boudalia, M.; Sekkat, Z.; Warad, I.; Guenbour, A.; Bellaouchou, A.; Zarrouk, A. Effect of alumina insertion on structural properties, thermal stability, and chemical durability of potassium calcium based-phosphate glasses. *Inorg. Chem. Commun.* **2022**, *142*, 109632, https://doi.org/10.1016/j.inoche.2022.109632.
39. Brow, R. K.; Tallant, D. R.; Myers, S. T.; Phifer, C. C. The short-range structure of zinc polyphosphate glass. *J. Non-Cryst. Solids* **1995**, *191*, 45-55, https://doi.org/10.1016/0022-3093(95)00289-8.
40. Pershina, S. v.; Antonov, B. D.; Leonidov, I. I. Effect of MoO_3 on structural, thermal and transport properties of lithium phosphate glasses. *J. Non-Cryst. Solids* **2021**, *569*, 120944, https://doi.org/10.1016/J.JNONCRYSOL.2021.120944.
41. Bartholomew, R. F. Structure and properties of silver phosphate glasses-infrared and visible spectra. *J. Non-Cryst. Solids* **1972**, *7*, 221-235, https://doi.org/10.1016/0022-3093(72)90024-5.
42. Alaoui, Y.; El Moudane, M.; Er-rafai, A.; Khachani, M.; Ghanimi, A.; Sabbar, A.; Tabyaoui, M.; Guenbour, A.; Bellaouchou, A. Structural study, thermal and physical properties of K_2O-CaO-P_2O_5 phosphate glasses. *Mor. J. Chem.* **2021**, *9*, 454-463, https://doi.org/10.48317/IMIST.PRSM/morjchem-v9i2.22505.
43. Julien, C. Local cationic environment in lithium nickel–cobalt oxides used as cathode materials for lithium batteries. *Solid State Ion.* **2000**, *136–137*, 887–896, https://doi.org/10.1016/S0167-2738(00)00503-8.
44. Julien, C. 4-volt cathode materials for rechargeable lithium batteries wet-chemistry synthesis, structure and electrochemistry. *Ionics* **2000**, *6*, 30–46, https://doi.org/10.1007/BF02375545.
45. Preudhomme, J.; Tarte, P. Infrared studies of spinels-II: The experimental bases for solving the assignment problem. *Spectrochim. Acta A Mol. Biomol. Spectrosc*. **1971**, *27*, 845–851, https://doi.org/10.1016/0584-8539(71)80163-0.
46. Guji, K. W.; Chien, W. C.; Wang, F. M.; Ramar, A.; Chemere, E. B.;Tiong, L.;Merinda, L. Lithium and Potassium Cations Affect the Performance of Maleamate-Based Organic Anode Materials for Potassium-and Lithium-Ion Batteries. *Nanomaterials* **2021**, *11*, 3120, https://doi.org/10.3390/NANO11113120.
47. Song, J.; Wu, D.; Zhang, C.; Ming, Q.; Imanzadeh, M. Investigation of mixed alkali effect on the DC electrical conductivity, structural, and physical properties of phosphate glasses containing MnO_2. *J. Phys. Chem. Solids* **2022**, *167*, 110759, https://doi.org/10.1016/j.jpcs.2022.110759.
48. Salem, S. M.; Abdel-Khalek, E. K.; Mohamed, E. A.; Farouk, M. A study on the optical, structural, electrical conductivity and dielectric properties of a lithium bismuth germanium tungsten glasses. *J. Alloys Compd.* **2012**, *513*, 35–43, https://doi.org/10.1016/J.JALLCOM.2011.09.052.
49. Boudad, L.; Taibi, M.; Belayachi, A.; Abd-Lefdil, M. Dielectric relaxation, electrical conductivity and optical studies of solid-state synthesized $EuCrO_3$. *J. Mater. Sci. Mater. Electron.* ***2020***, *31*, 354–360, https://doi.org/10.1007/S10854-019-02533-0.
50. Joshi, J. H.; Kanchan, D. K.; Joshi, M. J.; Jethva, H. O.; Parikh, K. D. Dielectric relaxation, complex impedance and modulus spectroscopic studies of mix phase rod like cobalt sulfide nanoparticles. *Mater. Res. Bull.* **2017**, *93*, 63–73, https://doi.org/10.1016/j.materresbull.2017.04.013.
51. Salem, S. M.; Antar, E. M.; Mostafa, A. G.; Salem, S. M.; El-Badry, S. A. Compositional dependence of the structural and dielectric properties of Li_2O-GeO_2-ZnO-Bi_2O_3-Fe_2O_3 glasses. *J. Mater. Sci.* **2011**, *46*, 1295–1304, https://doi.org/10.1007/S10853-010-4915-4.
52. Salem, S. M. Dielectric properties, conductivity, UV–visible and infrared spectroscopy of PbO P_2O_5 NaF glasses containing WO_3. *J. Non-Cryst. Solids* **2012**, *358*, 1410–1416, https://doi.org/10.1016/J.JNONCRYSOL.2012.03.020.
53. Elmoudane, M.; Et-tabirou, M.; Hafid, M. Glass-forming region in the system Li_3PO_4-$Pb_3(PO_4)_2$-$BiPO_4$ (Li_2O-PbO-Bi_2O_3-P_2O_5) and its ionic conductivity The glass-forming region in the system. *Mater. Res. Bull.* **2000**, *35*, 279-287, https://doi.org/10.1016/S0025-5408(00)00196-3.